*Article*

# AC/DC: The FERMI FEL Split and Delay Optical Device for Ultrafast X-ray Science

Alberto Simoncig [1,*], Michele Manfredda [1], Giulio Gaio [1], Nicola Mahne [2], Lorenzo Raimondi [1], Claudio Fava [1], Simone Gerusina [1], Riccardo Gobessi [1], Alessandro Abrami [1], Flavio Capotondi [1], Dario De Angelis [1], Ralf Hendrik Menk [1,3,4], Matteo Pancaldi [1], Emanuele Pedersoli [1] and Marco Zangrando [1,2]

[1] Elettra Sincrotrone Trieste S.C.p.A., Area Science Park, S.S. 14 km 163.5, 34149 Trieste, Italy; michele.manfredda@elettra.eu (M.M.); giulio.gaio@elettra.eu (G.G.); lorenzo.raimondi@elettra.eu (L.R.); claudio.fava@elettra.eu (C.F.); simone.gerusina@elettra.eu (S.G.); riccardo.gobessi@elettra.eu (R.G.); alessandro.abrami@elettra.eu (A.A.); flavio.capotondi@elettra.eu (F.C.); dario.deangelis@elettra.eu (D.D.A.); ralf.menk@elettra.eu (R.H.M.); matteo.pancaldi@elettra.eu (M.P.); emanuele.pedersoli@elettra.eu (E.P.); marco.zangrando@elettra.eu (M.Z.)

[2] Istituto Officina dei Materiali, CNR, Area Science Park, S.S. 14 km 163.5, 34149 Trieste, Italy; mahne@iom.cnr.it

[3] Istituto Nazionale di Fisica Nucleare, Sezione di Trieste, Via A. Valerio 2, 34127 Trieste, Italy

[4] Department of Medical Imaging, University of Saskatchewan, Saskatoon, SK S7N 5A2, Canada

[*] Correspondence: alberto.simoncig@elettra.eu

**Abstract:** Free-electron lasers (FELs) are the most advanced class of light-sources, by virtue of their unique capability to lase high-brightness pulses characterized by wavelengths spanning the extreme-ultraviolet, the soft and hard X-ray spectral domains, as well as by temporal lengths lying in the femtosecond (fs) timescale. The next step to push the current standards in ultrafast X-ray science is strongly linked to the possibility of engineering and exploiting time-resolved experiments exclusively for FELs pulses, ideally having different colors tunable at specific electronic resonance of the chemical elements. At the seeded FERMI FEL (Trieste, Italy) this goal is committed to the optical device known as AC/DC, which stands for the auto correlator/delay creator. AC/DC is designed to double the incoming FEL pulse splitting the photon beam by inserting a grazing incidence flat mirror, thus preserving the spectral and temporal properties, and further delaying one of these two pulses in time. It can independently tune the FEL pulses fluence on the two optical paths by means of solid-state filters, too. Here, we present a detailed description about this optical device. Strong emphasis is dedicated to the AC/DC opto-mechanical design and to the laser-based feedback systems implemented to compensate for any mismatch affecting the FEL optical trajectory, ascribable to both mechanical imperfections and paraxial errors rising during a temporal delay scan.

## 1. Introduction

Free-electron lasers (FELs) are the most advanced class of light-sources by virtue of their unique capability to lase high-brightness and ultrashort pulses. Indeed, their wavelengths cover an extremely large spectral domain, nowadays easily spanning the extreme ultra-violet (EUV), the soft (SXR) and the hard X-ray (HXR), along with pulse temporal lengths lying in the femtosecond (fs) timescale [1]. The first FELs operating at these wavelengths were based on the self-amplified spontaneous emission (SASE) process, i.e., on the generation of light pulses rising from the stochastic amplification of the radiation spontaneously emitted by an electron bunch wiggling inside an undulator device [1,2]. Although the SASE-based FELs can easily lase extremely high-brightness radiation, their pulses suffer from several limitations, mainly ascribable to the intrinsic stochastic nature of the SASE process, as well as to the lack of any resonant cavity in the machine layout,

resulting in significant shot-to-shot pointing and intensity instabilities, lack of spectral purity, and thus requiring complex synchronization systems combined with external laser sources to perform time-resolved spectroscopies [3–6].

The FERMI FEL, based on the external laser seeding scheme, and located at the Elettra Sincrotrone Trieste premises (Italy), set new standards in terms of EUV/SXR pulses emission [7]. Specifically, FERMI is a single-pass FEL light-source able to lase nearly transform-limited and fully coherent pulses between 100 nm and 4 nm (in first harmonic), alongside having full control of the radiation polarization state too [8]. Based on these almost unique features, several spectroscopical methods, employed daily at synchrotron light-sources, such as X-ray absorption (XAS), linear and circular magnetic dichroism (XMLD/XMCD) and resonant inelastic scattering (RIXS), were extended into the time-domain. Moreover, the advent of fully coherent radiation sources, such as FERMI, has allowed pushing non-linear optical spectroscopies, normally exploited exclusively at table-top light-sources in the infrared (IR) or optical regimes, into the EUV/SXR wavelengths [9–12]. Nonetheless, the next step to push the current standards in ultrafast X-ray science is strongly constrained by the possibility of designing and performing time-resolved experiments exclusively engaging EUV, SXR and HXR pulses. Indeed, exciting (and probing) matter at (nearby) its electronic resonance is widely speculated to be the key for discriminating and hopefully revealing mechanisms hiding behind some of the most exotic behavior of physical, chemical and biological systems. This calls for designing new optical devices capable of (i) splitting the incoming pulses, preserving their unique spectral and temporal features; (ii) transmitting and filtering an acceptable fluence; (iii) delaying one of these pulses in time; and finally, (iv) keeping the focal spots positions (in the focal plane inside the experimental end station) overlapped at an almost zero cost in term of pointing and temporal jitters. These kinds of optical devices are currently under development (or already commissioned) in several FELs and high-order harmonic generation (HHG) light-sources [13–15].

Specifically, in the FERMI FEL, these requirements are addressed by an ad hoc optical device installed along the Photon Analysis Delivery and Reduction System (PADReS), accessible to three experimental end-stations (DiProI, LDM, EIS-Timex), and known as AC/DC which stands for auto correlator/delay creator [16]. AC/DC is designed to split the incoming FEL photon beam by inserting a grazing incidence flat mirror to create two exact half-spots. Subsequently, these are made to travel along two different optical paths, the first one featuring a fixed-length, while the second one is characterized by a variable-length, which can be tuned by moving the relative longitudinal positions of two grazing incidence mirrors mounted onto two specular mechanical rails (see Figure 1). In this way, it is possible to introduce a tunable temporal delay ($\Delta\tau$) between these two EUV/SXR pulses and address the possibility of performing time-resolved experiments within a FEL-FEL configuration. Moreover, AC/DC allows for polychromatic time-resolved FEL-FEL experiments characterized by non-degenerate pump and the probe radiations, i.e., tuned at different wavelengths. Indeed, thanks to the double cascade scheme of FERMI (FEL2 layout), where two FEL pulses with different colors are generated, in addition to the use of selective solid-state filters inside the AC/DC, two delayed FEL pulses with different colors can be delivered to the experimental end-station to perform multidimensional spectroscopy studies [17].
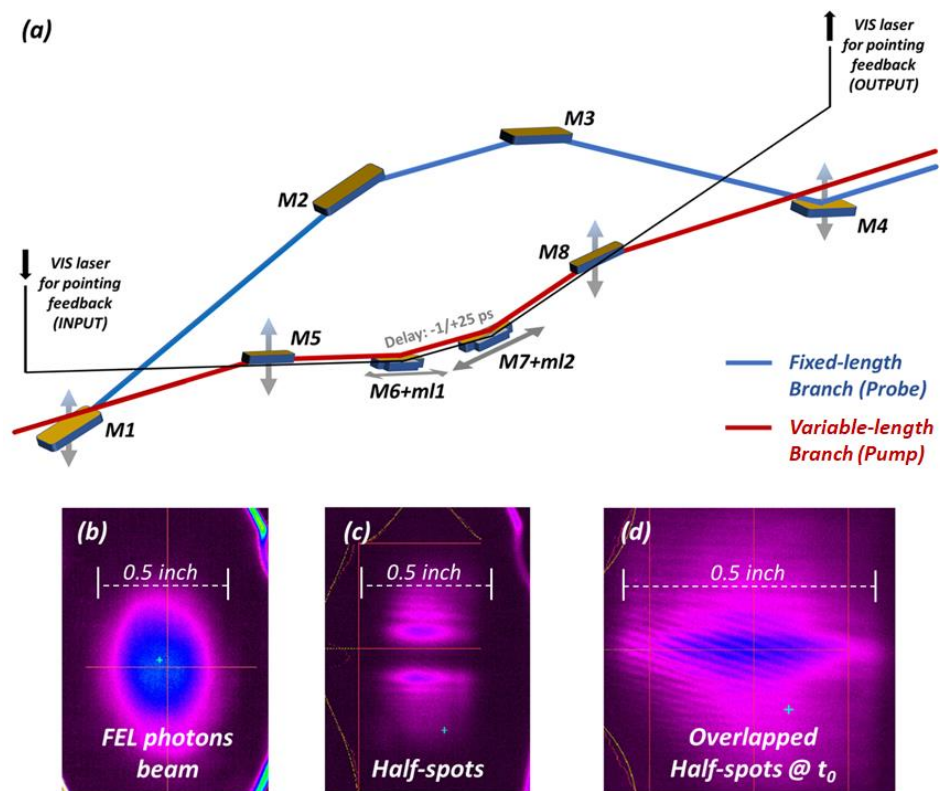
**Figure 1.** (**a**) Sketch of the AC/DC. Distances, dimensions and mirrors' incidence angles are reported out of scale for the sake of clearness. The incoming beam is split into two exact half-spots. The pulses reflected by M1 are steered into the (upper) fixed-length optical branch (blue line) and act as probe radiation. Instead, the ones straightly propagating after M1, enter the (lower) variable-length optical branch (red line), and become the pump beam. M6 and M7 can travel in a synchronous way, along a couple of specular mechanical rails to insert the desired temporal delay. The black line refers to the optical laser, which mimics the pump beam trajectory that is used to pick up all instabilities arising during the temporal scan, and thus it acts as a feedback signal to correct any potential misalignment. To do this, the VIS laser beam is reflected by two mirrors (ml1 and ml2) installed alongside M6 and M7; (**b**) the FEL photons beam on a Ce:YAG screen at the far-field without the AC/DC; (**c**) the two FEL half-spots on the same Ce:YAG screen with the AC/DC; (**d**) the two FEL half-spots overlapped in space and time at $t_0$, this last one being identified by looking at the appearance of interference fringe.

## 2. Materials and Methods

AC/DC is composed of four different units (see Figure 1a for a schematic of the AC/DC delay unit and Figure 2 for a more detailed view of its different mechanical components), which are (i) the first grazing incidence mirror (M1), designed to split the incoming FEL photons beam into two exact half-spots; (ii) the two, fixed- and variable-length optical branches (see blue and red lines in Figure 1a); (iii) the grazing incidence mirror (M4) aimed at recombining the two half-spots in the far-field; and (iv) the laser-based pointing feedback system (see black line in Figure 1a), implemented to preserve the spots overlap at the focal plane of the experimental end-station.

Specifically, all eight EUV/SXR mirrors (M1 ÷ M8) in the AC/DC present a Si-substrate, an Au-coating, a flat profile with a tangential error ≤ 0.5 μrad (rms), a sagittal one ≤ 5 Å (rms) and a roughness ≤ 3 Å (rms) in 2D. The corresponding active areas are 350 mm × 20 mm, 330 mm × 20 mm and 230 mm × 20 mm, for the M1/M4 pair, the M2/M3 pair and for the M5 ÷ M8 set, respectively. M1 is mounted onto a vertical actuator (grey arrow below M1 in Figure 1a) to intercept the incoming FEL photons beam along the ordinary optical transport path and to split its quasi TEM$_{00}$ gaussian transverse intensity distribution (see Figure 1b) into two exact half-spots (see Figure 1c). Several

Ce:YAG screens, positioned downstream of M1, can be used for monitoring, in real-time, the splitting correctness. The radiation reflected by M1 is steered into the fixed-length optical branch (see blue line in Figure 1a). The grazing incidence angle for this first set of mirrors (M1 ÷ M4) is 2°. M4 is also mounted onto a vertical actuator (grey arrow below M4 in Figure 1a), which allows its complete extraction during ordinary FEL operations.
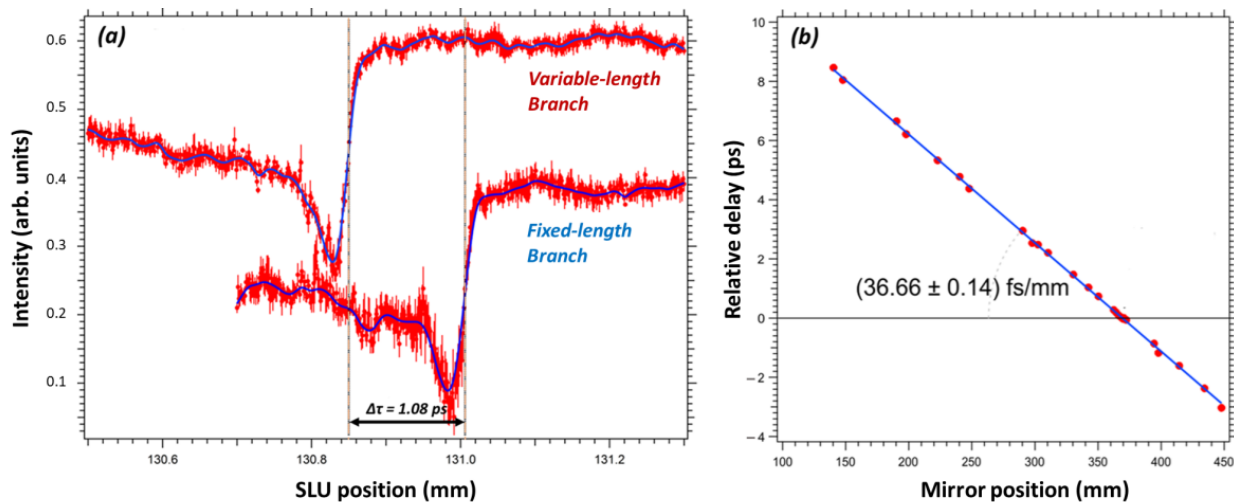


**Figure 2.** (**a**) $Si_3N_4$ optical transient reflectivity measured by means of a FEL (pump) and a SLU (probe) pulses. The two time-traces refer to the data acquired using the FEL pump beam travelling through the fixed-length branch, as well as the variable-length one. These datasets refer to a delay between the two FEL pulses equal to $\Delta\tau$ = +1.08 ps. (**b**) Linear dependence of $\Delta\tau$ vs. the M6/M7 positions, used for the AC/DC calibration.

The pulses propagated straight after M1 (not reflected) intercepted the second set of mirrors (M5 ÷ M8) installed at a grazing incidence angle of 3°. M5 and M8 are mounted on vertical actuators (grey arrows below M5/M8 in Figure 1a) in order to be easily removed for ordinary FEL operations. Once reflected by M5 the beam is steered towards M6 and M7, which can travel along a couple of specular mechanical rails to insert the desired amount of temporal delay (see red line in Figure 1a). M8 is designed to intercept the beam emerging from the fixed-length optical branch and to steer it towards the experimental end-station. The routine exact synchronization between the optical branches, can easily be performed by steering and overlapping the two FEL beams onto one of the Ce:YAG screens installed (≈20 m) downstream of the AC/DC, and scanning the temporal delay $\Delta\tau$ in the proximity of the expected value until an interference fringe appears (see Figure 1d), setting the time-zero ($t_0$) for the time-resolved experiment at their maximum signal. This is done by acting on the angular degrees of freedom of M4 and M8, while the $\Delta\tau$ is controlled by means of the longitudinal positions of M6 and M7 (see Figure 1). The accessible $\Delta\tau$ varies between −1 and ≈+26 picoseconds (ps).

Instead, the first AC/DC start-up required a more delicate operation to properly characterize the relation existing between the M6/M7 longitudinal positions and the corresponding $\Delta\tau$. Indeed, each EUV/SXR beam propagating through a single AC/DC optical branch can be used as standalone pump radiation if coupled to a proper optical probe. For the latter, the easiest choice is the near-infrared (NIR) laser available at each experimental end-station, i.e., the seed-laser for users (SLU). Such a laser beam is the residual part of the fundamental Ti:sapphire emission of the seeding amplifier, i.e., not used for the machine seeding process, which is propagated (in vacuum) towards the FERMI experimental hall at a cost of a timing jitter of a few fs [18]. To quantify this jitter, both FEL and NIR pulses have been focused onto a (free-standing) silicon nitride ($Si_3N_4$) membrane, the former pumping this sample, with the latter probing how its optical reflectivity varies at the arrival of the FEL radiation. Indeed, at the coincidence arrival time

between the FEL and the NIR pulses, a large change of the sample reflectivity is discernible (see Figure 2a). By measuring the $Si_3N_4$ transient reflectivity engaging the FEL beam propagating through the fixed-length optical branch as a pump radiation, it is possible to fix the exact coincidence arrival time between the FEL and NIR pulses. Similarly, it is possible to perform the same measurement using the FEL radiation propagating through the variable-length optical branch, too. Later, by varying the longitudinal positions of the M6/M7 pair, it is possible to link these coordinates to the temporal delay ($\Delta\tau$) by comparing the shift in time between the two $Si_3N_4$ transient reflectivity datasets. The M6/M7 longitudinal positions vs. $\Delta\tau$ shows a linear dispersion, and the angular coefficient returns the relation existing between the amount of mechanical delay and the temporal one, which is estimated to be $36.66 \pm 0.14$ fs/mm (see Figure 2b). Since the mechanical resolution of the M6/M7 longitudinal actuators is of 10 microns the corresponding AC/DC temporal resolution is $\approx$360 as.

Within this layout, the beam reflected by M1 and steered by the fixed-length optical branch acts to probe the samples under investigation, while the one, whose trajectory is defined by the variable-length optical branch, is used as the pump radiation. Such a choice is dictated by the will to preserve the pointing probe completely unaffected by any vibrations, which could arise during the temporal scan. All mirrors are mounted into three different ultra-high vacuum (UHV) chambers (see Figure 3), constantly kept at a value approximately in the $10^{-9}$ mbar range and installed onto concrete supports to dampen the vibrational noise coming from the external environment. Specifically, M1 and M4 are mounted into two separate bell-shape UHV chambers, while the other mirrors composing the proper delay unit are installed inside an intermediate and separate UHV chamber.
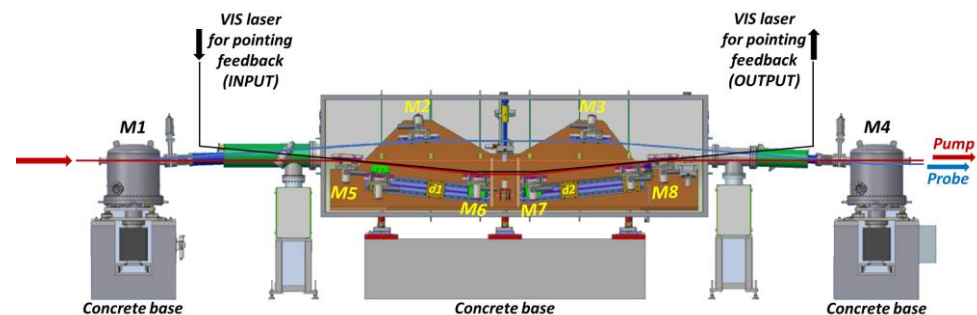


**Figure 3.** AC/DC mechanical design (side-view). All mirrors and actuators are enclosed into three different UHV chambers. These are all mounted on concrete bases to dampen the vibrations coming from the external environment.

Figure 4 depicts the overall AC/DC transmission in the nominal operation range of FERMI. Between 10 nm and 100 nm radiation wavelength, the fixed-length optical branch transmits approximately $0.8 \div 0.9$ of the incoming radiation intensity. Instead, the variable-length optical branch, due to the higher grazing incidence angles, exhibits a slightly lower efficiency lying in the range of $0.7 \div 0.85$. Below 10 nm wavelength, the efficiency of both optical branches drastically drops and exhibits similar qualitative results (50%) at 6 nm, and 35% (fixed-length branch) and 20% (variable-length branch) at 4 nm, respectively. Calculations are performed by means of Weaver's optical constants database for wavelengths greater than 40 nm, implemented within David Windt's code, and using the online CXRO database for the other domain, where solid and dashed lines refer to the transmission efficiency of the two optical branches for different polarization (S and P), respectively [19,20].
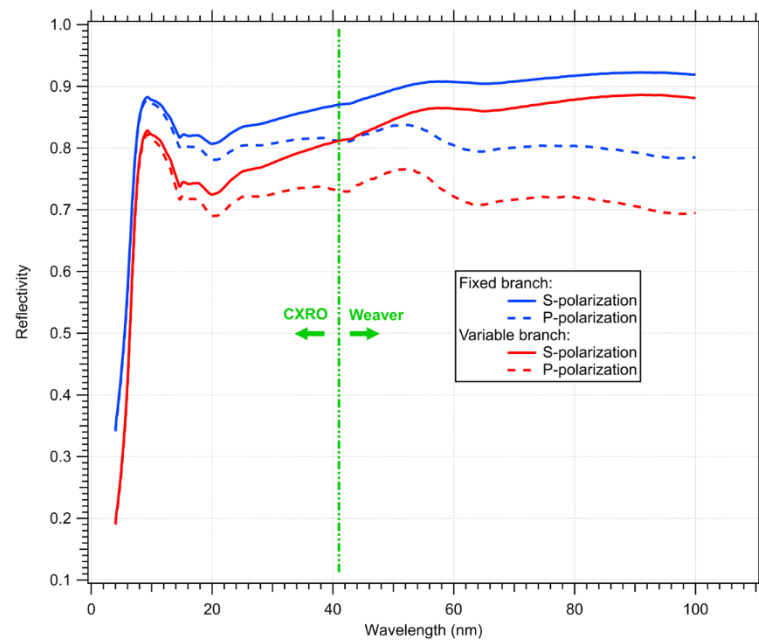
**Figure 4.** Calculated AC/DC reflectivity. Blue and red lines refer to the fixed-length and variable-length optical branch, respectively.

## 3. Results

### 3.1. Alignment

Once the beam splitting and the temporal synchronization are properly achieved, the two outcoming beams are steered towards the end-stations. Here, they are focused and recombined by means of the focusing optics, which are the KAOS active Kirkpatrick-Baez optical system on DiProi and LDM, and a fixed-curvature bulk ellipsoidal mirror (Carl Zeiss STM GmbH, Oberkochen, Germany) on EIS-TIMEX [21–23]. The overlap at the focal plane is achieved first by making the two beams exiting the AC/DC coarse-grain parallel to each other, then by finalizing the overlap by monitoring the spot position directly at the focal plane (see Figure 5a,b). In doing so, the horizontal and vertical pointing of the trajectories is controlled via pitch and roll angles of the M4/M8 mirrors, while the observation is performed on three scintillator screens (Ce:YAG) along the transport and on one scintillator in the experimental chamber. Notice that linear actuators containing filters and beam stoppers, mounted just $\approx 1$ m downstream of the AC/DC, can be used to balance the intensities or to select just one of the two pulses. All three of these focusing optical devices are designed to deliver high de-magnification rates (from 60 to 80 times depending on the FEL configuration used), thereby achieving, at the shortest wavelengths of FERMI, an FWHM-spot size down to a few microns in the focal plane. Therefore, to preserve an acceptable spatial overlap in the end-station experimental chamber, a pointing stability of the order of $\approx 1 \div 2$ microns must be preserved during the whole temporal scan of the AC/DC. This is especially challenging when the AC/DC is spanning the time delay over the whole accessible range, which requires synchronously moving the M6/M7 pair along the whole accessible length of the rails (see *d*1, *d*2 in Figure 3), which are each approximately 800 mm long. During this operation, the pointing is affected by factors such as: (i) insufficient mechanical tolerance, (ii) vibrations of the mirror holders and (iii) thermal expansion. The entity of such effects is such that the overlap is typically disrupted at $\Delta\tau \approx 10$ ps (see Figure 5c). Such an issue would greatly reduce the performance of the AC/DC, thus it has been addressed by developing a hybrid opto-numerical laser feedback system.
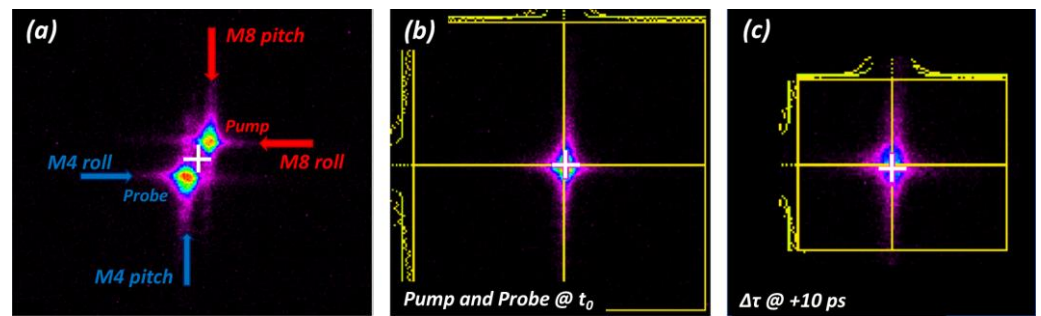
**Figure 5.** (**a**) Spots at the focal plane in the experimental end-station. To obtain the proper overlap, both pump and probe spots are steered towards their center of mass (white cross target) by acting on the pitch and roll actuators of M4/M8. (**b**) Overlapped spots at $t_0$, and (**c**) pump spot position at a delay of +10 ps, operating (on purpose) the feedback without any numerical correction to the effective pointing target. In this case, it is possible to observe a slight offset, more pronounced along the vertical axis, ascribable to residual paraxial errors.

### 3.2. Pointing Instability and Feedback System

Alongside the FEL pump, i.e., the beam travelling through the variable-length optical branch, we propagate a visible (VIS) laser beam to mimic the FEL trajectory. This laser is inserted into the AC/DC by means of an optical breadboard mounted onto an external (in air) separate holder (see Figure 6a) and holding a laser diode coupled to an optical fiber (1), whose radiation is magnified by an out-coupler device (2) and steered into the AC/DC by commercial Ag-coated 1-inch laser mirrors (3). Two optical mirrors (ml1 and ml2 in Figure 1a) are placed nearby M6/M8, which present Si-substrates, Ag-coating and an active area of 100 mm × 15 mm. The coplanarity between the M6/M7 and their corresponding laser mirrors (ml1/ml2) has been checked ex situ by means of a phase shifting Fizeau interferometer. In this way, the VIS laser beam propagates parallelly along the FEL optical path defined by M5 ÷ M8, and any deflection of the trajectory of the FEL beam (induced by the photon transport inside the AC/DC) equally affects the pointing of the laser beam. After the reflection from ml2, the laser beam exits the AC/DC through a viewport and propagates towards an external detection breadboard (see Figure 6b), where it is focused by means of a lens (4) (focal length of 1.5 m) and further steered onto a naked, i.e., without any additional objective, CCD (5) camera (Basler AG, Ahrensburg, Germany). Such a detector monitors, in real time, the VIS beam position (see Figure 6c). Since the VIS laser shares the same optical path with the FEL pulses, any systematic distortion affecting the photon transport into the variable-length optical branch also modifies the position of the VIS laser beam on the CCD camera. In order to counteract any displacement due to mechanics, a real time feedback, integrated in the FERMI control system, estimates the position of the centroid of the VIS laser beam spot acquired by the CCD camera and keeps it fixed by changing the pitch and roll positions of the M7 through piezo (PI-Physik Instrumente GmbH, Karlsruhe, Germany) actuators (see Figure 6d).

Nonetheless, the laser-based optical feedback is not sufficient to fully compensate the position errors in the FEL pointing for the entire accessible Δτ range. Although the coplanarity of the ml1/M6 pair and the ml2/M7 one has been checked ex situ, any mechanical and thermal vibration affecting these holders during the installation inside the main UHV chamber, as well as the first pumping operation, cause a nonnegligible paraxial error. The result of this error, that cannot be compensated by the optical feedback system, is a residual offset between the two FEL spots, which is more evident when Δτ is larger than 10 ps and the focusing in the experimental end-station is extremely tight (few µm sizes).

To overcome this limitation, an ad hoc opto-numerical feedback system was designed, replacing the raw estimation of the VIS laser beam spot position with a virtual spot which is the sum of the VIS laser beam spot plus a correction factor that (linearly) depends on Δτ. To estimate such a correction factor at a few Δτ positions, an out of loop CCD camera measures, keeping the optical feedback retained in an active state, the displacement of the FEL focal

spot compared to the one coming from the fixed-length optical branch at established Δτ values (see Figure 5c). For each of these Δτ values a simplex-based optimization algorithm (Nelder-Mead) automatically modifies the linear coefficients of the correction factor valid for that delay till the feedback, reacting to the new correction factor applied to the real spot position, returns the FEL spot to the reference target. Once this procedure is completed, the position returned by the virtual spot algorithm of the overall Δτ range is a simple linear interpolation between these calibrated positions.
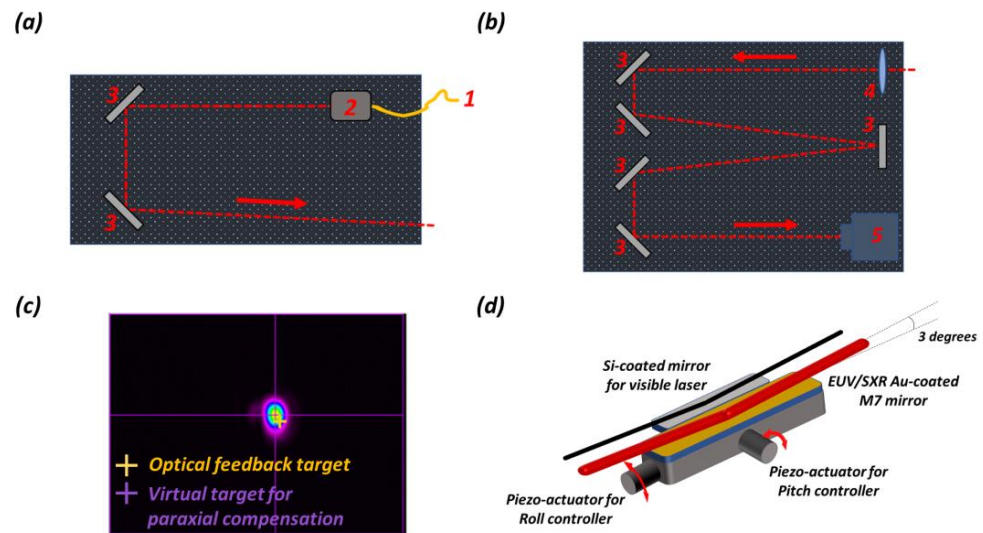


**Figure 6.** Optical breadboards are built to (**a**) steer the VIS laser beam into the AC/DC, and (**b**) monitor its beam position at the exit of the AC/DC. The red arrows refer to the VIS laser beam path. (**c**) Visible laser spot on the CCD detector. The yellow cross refers to the optical feedback target, while the violet one represents the effective target position when the hybrid opto-numerical algorithm is activated. (**d**) Sketch of the M7 mirror holder. The Au-coated EUV/SXR mirror is mounted next to an Ag-coated laser mirror. The entire holder hosts piezo actuators for modifying the pitch and roll position depending on the feedback signal.

From a quantitative point of view, the laser feedback reduces the overall instability affecting the position of the spots (within the focal plane) compatible with the vibrational noise affecting the experimental end-stations. This behavior is emphasized in the temporal sequence shown in Figure 7, where the position of the probe spot (at the focal plane) is shown at four different Δτ, starting from $t_0$ up to the end of the mechanical rails, i.e., at +24 ps and +26 ps, in addition to the half range position at +12 ps. The white cross is the reference target, while the spot sizes are in the range of 10 microns (FWHM). On the other hand, it is useful to underline that the lack of any dedicated pointing system, i.e., kept in a stand-by condition, is marked by a pointing error of the order of 100 higher than the corrected one, therefore precluding the use of extremely narrow focusing.



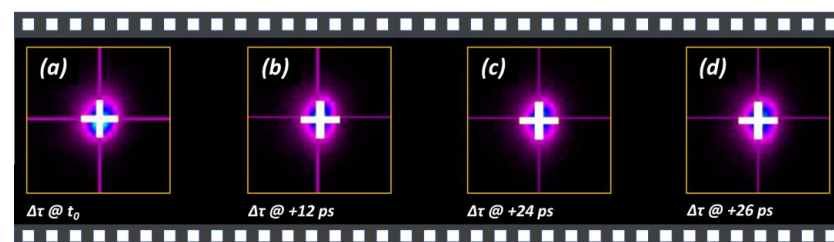**Figure 7.** Temporal sequence of the pump focus position at four different delays (Δτ), keeping the feedback pointing system activated, specifically at (**a**) $t_0$, (**b**) the half range at Δτ = +12 ps, and at end of the mechanical rails (**c**) at Δτ = +24 ps and (**d**) Δτ = +26 ps. The white cross refers to the desired target position. The estimated spot sizes are ≈10 μm (FWHM).

### 3.3. Fringe Stability

Whereas the feedback-system compensates for the pointing instability due to the change of the temporal delay, there is still another class of disturbances that cannot be counterweighted as effectively. It consists of the environmental vibrations affecting the mechanics and of the pointing instability of the FEL source, both of which eventually translate into fluctuations of the optical path lengths. Such spatial (and thus temporal) jitter generates shot-to-shot fluctuations of the fringe position, which can be appreciated, i.e., by observing the interference pattern with a fast, high-resolution detector.

Figure 8a displays the fringe system acquired at a repetition rate of 50 Hz by a prototype back illuminated scientific CMOS camera, which has been developed in collaboration between PCO (PCO AG, Donaupark 11, 93309 Kelheim, Germany) and Elettra Sincrotrone Trieste [24]. The CMOS camera was placed 750 mm downstream of the nominal focal plane of the DiProI end-station, at $t_0$. The spot size and shape are ad hoc tailored by means of KAOS, and the M4/M8 pair are tuned to preserve the spatial overlap between the spots. Figure 8b shows a stack of $\approx 4000$ profiles in the fringe pattern, where each profile (displayed in a row) is taken within the dashed line of panel (a). The horizontal shift of each fringe profile with respect to an arbitrary reference (black line in the Figure 8b plot), is due to the sought temporal jitter. The maximum fringe shift is of the order of $\pm \lambda/2$, which at the FEL wavelength of $\lambda = 17.8$ nm corresponds to $\approx 60$ as. Figure 8c/d display the comparison between a single-shot image and the numerical summation of 3700 images: the fringe visibility is reduced by a factor $\approx 5$, but is still visible. This suggests that integrated measurements are, in general, an accurate balance between the acquisition time and the characteristic time of visibility reduction (which is revealing of the temporal jitter between the two branches) is found. Further delving into the statistics of fringe jitter, it turns out that the histogram of phase jitters (expressed in $\lambda$) reveals a non-Gaussian distribution, exhibiting two marginal density peaks with a FWHM of $\approx \lambda/5$ (left) and $\approx \lambda/3$ (right) (see Figure 8e). Such a bi-stable distribution, resembling those of oscillatory phenomena, can be revealing of low-frequency vibrations either in the mechanical components or, more intriguingly, in the beam trajectory delivered by the machine. In this perspective, after an appropriate championing for the characterization of environmental disturbances, the AC/DC would represent an excellent candidate for investigating, with high sensitivity, the correlation between possible machine operation parameters and the beam stability.
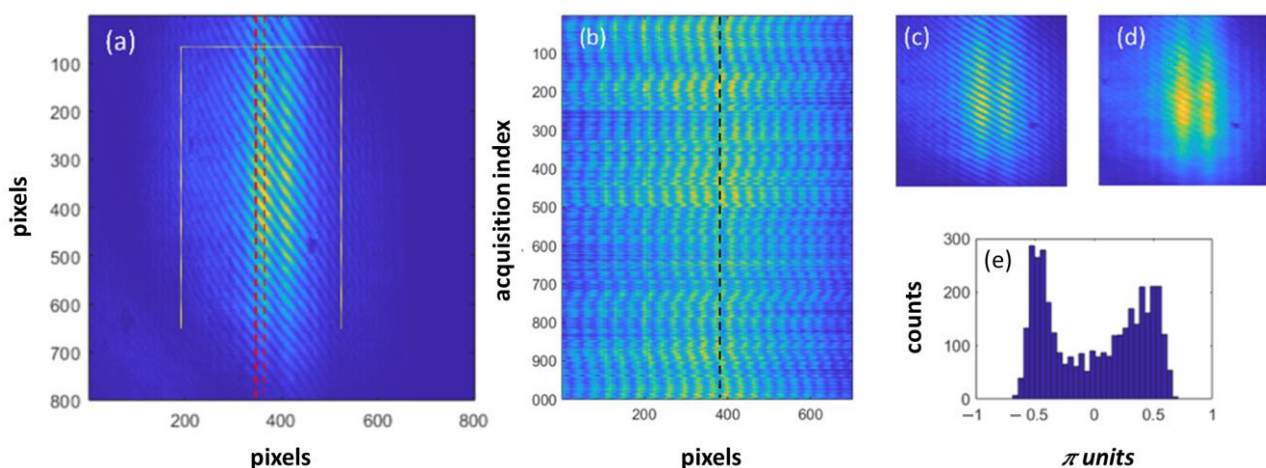


**Figure 8.** (**a**) Out-of-focus, single shot acquisition (at DiProI) at $t_0$. (**b**) Stack of vertical profiles computed within the red region-of-interest of panel (**a**). Each profile deploys horizontally; black line: arbitrary reference. (**c**,**d**) Details of the yellow region-of-interest of panel (**a**) displaying a single shot and a numerically averaged image (over 3700 shots), respectively. (**e**) Histogram of the fringe displacement jitter, expressed in $\pi$ units.

### 3.4. The Time-Dependent Amplitude-Autocorrelation

In terms of FEL source metrology, the AC/DC provides an immediate user-friendly way to assess one of the still-debated quantities in the FEL community, that is the longitudinal coherence length of the FEL pulses. Indeed, to date a lot of effort has been dedicated to the full characterization of FELs' pulse temporal structure, whose ultimate duration (at SASE FELs) is now reported to break the fs barrier, i.e., paving the way towards as spectroscopies at large-scale facilities [5,6,25–27].

Specifically, at FERMI, the issue of the longitudinal coherence length can be addressed either looking at the fringe in the experimental chambers (i.e., after the focusing), or along the transport. Here we report the results obtained in the first configuration, with the setup described in the previous section, by taking advantage of KAOS to conveniently shape the spot to the detection camera used. Figure 9a reports the visibility of fringes as a function of $\Delta\tau$, and data refer to two different FEL wavelengths, where dots refer to the experimental points (each point is the average over 5 seconds, i.e., 250 shots) and solid lines represent the Gaussian fit. It turns out that the coherence length, computed as the full width half maxima (FWHM) of the Gaussian fit, divided by $\sqrt{2}$ to consider the autocorrelation effect, is $\ell_C = 66.5$ fs for a dispersive current for the FEL wavelength set at 41.6 nm, and $\ell_C = 47.5$ fs for the machine tuned at 17.8 nm. The coherence length provides a lower limit to the estimation of the longitudinal pulse length $\ell_P$, i.e., $\ell_C \leq \ell_P$, where the equality holds for Fourier-transformed pulses. The corresponding FEL pulse spectra, detected by means of the PRESTO high-resolution online spectrometer ($\Delta\lambda/\lambda \sim 10^{-4}$), are reported in Figure 9b,c, and exhibit an FWHM shrinking of approximately 25% when the wavelength is tuned from 41.6 to 17.8 nm [15]. In this perspective, the AC/DC, combined with the existing instrumentation at FERMI, candidates as a valuable instrument for the further characterization of machine performance in the view of more accurate experiment planning and of the facility upgrades.
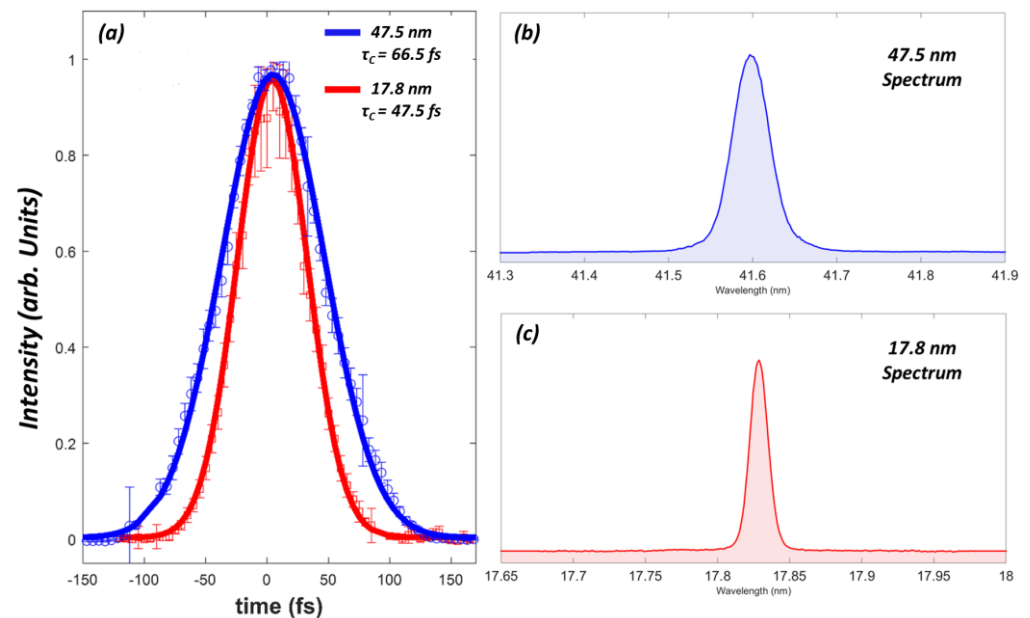


**Figure 9.** (**a**) Visibility of fringes as function of $\Delta\tau$, captured at two different values for the current of the machine dispersive section. (**b**,**c**) Corresponding spectra.

## 4. Conclusions

We presented a detailed report about the optical device known as AC/DC, installed along the FERMI FEL optical transport (PADReS), and purposely designed to allow performing time-resolved spectroscopies exclusively engaging EUV/SXR pulses as pump and probe, with an intrinsic temporal resolution of $\approx$360 as. We dedicated a strong emphasis to the description of the AC/DC opto-mechanical design, as well as on ad hoc laser-based

pointing system, which combines the physical signal acquired by monitoring the position of the laser beam, that mimics the FEL beam trajectory traveling in the variable-length optical branch, and a dedicated algorithm to correct any residual paraxial errors. To conclude, we presented a brief overview of some preliminary results which emphasize the possibilities that the AC/DC offers to the users to implement novel spectroscopical layouts.

**Author Contributions:** Conceptualization, A.S., M.M., L.R., N.M., C.F., S.G., R.G. and M.Z.; methodology, C.F., S.G., R.G., A.S., M.M., L.R., N.M., G.G., A.A. and M.Z.; software, M.M., E.P., M.P., R.H.M., G.G. and A.A.; validation, A.S., M.M., L.R., N.M., F.C., E.P., M.P., D.D.A., G.G. and M.Z.; formal analysis, A.S., M.M., L.R., N.M., F.C., E.P., M.P., D.D.A., G.G. and M.Z.; investigation, A.S., M.M., L.R., N.M., F.C., E.P., M.P., D.D.A., G.G. and M.Z.; resources, C.F., S.G., R.G., R.H.M., G.G., A.A. and M.Z.; data curation, A.S., M.M., L.R., N.M., F.C., E.P., M.P., D.D.A. and M.Z.; writing—original draft preparation, A.S., M.M., G.G., F.C. and M.Z.; writing—review and editing, A.S., M.M., L.R., N.M., R.H.M., D.D.A., G.G., F.C. and M.Z.; visualization, A.S., M.M., N.M., F.C. and M.Z.; supervision, M.Z.; project administration, M.Z. All authors have read and agreed to the published version of the manuscript.

## References

1. Pellegrini, C.; Marinelli, A.; Reiche, S. The physics of x-ray free electron lasers. *Rev. Mod. Phys.* **2016**, *88*, 015006. [CrossRef]
2. Bostedt, C.; Boutet, S.; Fritz, D.M.; Huang, Z.; Lee, H.J.; Lemke, H.T.; Robert, A.; Schlotter, W.F.; Turner, J.J.; Williams, G.J. Linac Coherent Light Source: The first five years. *Rev. Mod. Phys.* **2016**, *88*, 015007. [CrossRef]
3. Schreiber, S. First Lasing at 32 nm of the VUV-FEL at DESY. In Proceedings of the 27th International Free Electron Laser Conference (FEL 2005), Stanford, CA, USA, 21–26 August 2005; pp. 12–18.
4. Chalupský, J.; Krzywinski, J.; Juha, L.; Hájková, V.; Cihelka, J.; Burian, T.; Vyšín, L.; Gaudin, J.; Gleeson, A.; Jurek, M.; et al. Spot size characterization of focused non-Gaussian X-ray laser beams. *Opt. Express* **2010**, *18*, 27836. [CrossRef] [PubMed]
5. Grguraš, I.; Maier, A.R.; Behrens, C.; Mazza, T.; Kelly, T.J.; Radcliffe, P.; Düsterer, S.; Kazansky, A.K.; Kabachnik, N.M.; Tschentscher, T.; et al. Ultrafast X-ray pulse characterization at free-electron lasers. *Nat. Photonics* **2012**, *6*, 852. [CrossRef]
6. Schulz, S.; Grguras, I.; Behrens, C.; Bromberger, H.; Costello, J.T.; Czwalinna, M.K.; Felber, M.; Hoffmann, M.C.; Ilchen, M.; Liu, H.Y.; et al. Femtosecond all-optical synchronization of an X-ray free-electron laser. *Nat. Commun.* **2015**, *6*, 5938. [CrossRef]
7. Allaria, E.; Appio, R.; Badano, L.; Barletta, W.A.; Bassanese, S.; Biedron, S.G.; Borga, A.; Busetto, E.; Castronovo, D.; Cinquegrana, P.; et al. Highly coherent and stable pulses from the FERMI seeded free-electron laser in the extreme ultraviolet. *Nat. Photonics* **2012**, *6*, 699–704. [CrossRef]
8. Allaria, E.M.; Diviacco, B.; Callegari, C.; Finetti, P.; Mahieu, B.; Viefhaus, J.; Zangrando, M.; De Ninno, G.; Lambert, G.; Ferrari, E.; et al. Control of the Polarization of a Vacuum-Ultraviolet, High-Gain, Free-Electron Laser. *Phys. Rev. X* **2014**, *4*, 41040. [CrossRef]
9. Allaria, E.M.; Battistoni, A.; Bencivenga, F.; Borghes, R.; Callegari, C.; Capotondi, F.; Castronovo, D.; Cinquegrana, P.; Cocco, D.; Coreno, M.; et al. Tunability experiments at the FERMI@Elettra free-electron laser. *New J. Phys.* **2012**, *14*, 113009. [CrossRef]
10. Dell'Angela, M.; Hieke, F.; Malvestuto, M.; Sturari, L.; Bajt, S.; Kozhevnikov, I.V.; Ratanapreechachai, J.; Caretta, A.; Casarin, B.; Glerean, F.; et al. Extreme ultraviolet resonant inelastic X-ray scattering (RIXS) at a seeded free-electron laser. *Sci. Rep.* **2016**, *6*, 38796. [CrossRef]
11. Prince, K.C.; Allaria, E.; Callegari, C.; Cucini, R.; de Ninno, G.; di Mitri, S.; Diviacco, B.; Ferrari, E.; Finetti, P.; Gauthier, D.; et al. Coherent control with a short-wavelength free-electron laser. *Nat. Photonics* **2016**, *10*, 176–179. [CrossRef]
12. Principi, E.; Krylow, S.; Garcia, M.E.; Simoncig, A.; Foglia, L.; Mincigrucci, R.; Kurdi, G.; Gessini, A.; Bencivenga, F.; Giglia, A.; et al. Atomic and electronic structure of solid-density liquid carbon. *Phys. Rev. Lett.* **2020**, *125*, 155703. [CrossRef] [PubMed]
13. Lu, W.; Friedrich, B.; Noll, T.; Zhou, K.; Hallmann, J.; Ansaldi, G.; Roth, T.; Serkez, S.; Geloni, G.; Madsen, A.; et al. Development of a hard X-ray split-and-delay line and performance simulations for two-color pump-probe experiments at the European XFEL. *Rev. Sci. Instrum.* **2018**, *89*, 063121. [CrossRef] [PubMed]

14. Roseker, W.; Hruszkewycz, S.O.; Lehmkühler, F.; Walther, M.; Schulte-Schrepping, H.; Lee, S.; Osaka, T.; Strüder, L.; Hartmann, R.; Sikorski, M.; et al. Towards ultrafast dynamics with split-pulse X-ray photon correlation spectroscopy at free electron laser sources. *Nat. Commun.* **2018**, *9*, 1704. [CrossRef] [PubMed]

15. Mandal, A.; Sidhu, M.S.; Rost, J.M.; Pfeifer, T.; Singh, K.P. Attosecond delay lines: Design, characterization and applications. *Eur. Phys. J. Spec. Top.* **2021**, *230*, 4195. [CrossRef]

16. Zangrando, M.; Cudin, I.; Fava, C.; Gerusina, S.; Gobessi, R.; Godnig, R.; Rumiz, L.; Svetina, C.; Parmigiani, F.; Cocco, D. First Results from the Commissioning of the FERMI@Elettra Free Electron Laser by Means of the Photon Analysis Delivery and Reduction System (PADReS). *Proc. SPIE* **2011**, *8078*, 80780I.

17. Allaria, E.; Bencivenga, F.; Borghes, R.; Capotondi, F.; Castronovo, D.; Charalambous, P.; Cinquegrana, P.; Danailov, M.B.; de Ninno, G.; Demidovich, A.; et al. Two-colour pump–probe experiments with a twin-pulse-seed extreme ultraviolet free-electron laser. *Nat. Commun.* **2013**, *4*, 2476. [CrossRef]

18. Danailov, M.B.; Bencivenga, F.; Capotondi, F.; Casolari, F.; Cinquegrana, P.; Demidovich, A.; Giangrisostomi, E.; Kiskinova, M.P.; Kurdi, G.; Manfredda, M.; et al. Towards jitter-free pump-probe measurements at seeded free electron laser facilities. *Opt. Express* **2014**, *22*, 12869–12879. [CrossRef]

19. Weaver, J.H.; Krafka, C.; Lynch, D.W.; Koch, E.E. *Physics Data: Optical Properties of Metals, 18*; Fach-Iformation Zentrum: Karlsruhe, Germany, 1981.

20. Center for X-Rays Optics Database. Available online: https://henke.lbl.gov/optical_constants/ (accessed on 31 December 2021).

21. Raimondi, L.; Svetina, C.; Mahne, N.; Cocco, D.; Abrami, A.; de Marco, M.; Fava, C.; Gerusina, S.; Gobessi, R.; Capotondi, F.; et al. Microfocusing of the FERMI@Elettra FEL beam with a K-B active optics system: Spot size predictions by application of the WISE code. *Nucl. Instrum. Meth. A* **2013**, *710*, 131–138. [CrossRef]

22. Raimondi, L.; Svetina, C.; Mahne, N.; Cocco, D.; Capotondi, F.; Pedersoli, E.; Kiskinova, M.; Keitel, B.; Brenner, G.; Ploenjes, E.; et al. K-B bendable system optimization at FERMI@Elettra FEL: Impact of different spatial wavelengths on the spot size. *Proc. SPIE* **2013**, *8848*, 63–70.

23. Manfredda, M.; Fava, C.; Gobessi, S.G.R.; Mahne, N.; Raimondi, L.; Simoncig, A.; Zangrando, M. The evolution of KAOS, a multipurpose active optics system for EUV/Soft X-rays. *Syn. Rad. News* **2022**. *accepted*.

24. Menk, R.H.; Arfelli, F.; Cautero, M.; Cautero, G.; di Fraia, M.; Coreno, M.; Galdenzi, F.; Tutsch, W. On the possibility to utilize a PCO Edge 4.2 bi scientific CMOS imager for extended ultra violet and soft X-ray photon detection. *JINST* **2022**, *17*, C01058. [CrossRef]

25. Capotondi, F.; Foglia, L.; Kiskinova, M.P.; Masciovecchio, C.; Mincigrucci, R.; Naumenko, D.; Pedersoli, E.; Simoncig, A.; Bencivenga, F. Characterization of ultrafast free-electron laser pulses using extreme-ultraviolet transient gratings. *J. Synchrotron Rad.* **2018**, *25*, 32. [CrossRef] [PubMed]

26. Hartmann, N.; Hartmann, G.; Heider, R.; Wagner, M.S.; Ilchen, M.; Buck, J.; Lindahl, A.O.; Benko, C.; Grünert, J.; Krzywinski, J.; et al. Attosecond time–energy structure of X-ray free-electron laser pulses. *Nat. Photonics* **2018**, *12*, 215. [CrossRef]

27. Ackermann, W.A.; Asova, G.; Ayvazyan, V.; Azima, A.; Baboi, N.; Bähr, J.; Balandin, V.; Beutner, B.; Brandt, A.; Bolzmann, A.; et al. Operation of a free-electron laser from the extreme ultraviolet to the water window. *Nat. Photonics* **2007**, *1*, 336–342. [CrossRef]